doi.org/10.36721/PJPS.2025.38.3.REG.13223.1

# Construction and characterization of thiolated chitosan coated TPGSylated nanodiamonds for oral delivery of curcumin

**Dandan Liu*[1], Zhiyuan Yang[1], Yue Lu[1] and Weiwei Yang[2]***
[1]School of Biomedical & Chemical Engineering, Liaoning Institute of Science and Technology, Benxi, Liaoning, China.
[2]Health Management Center, Baoji Central Hospital, Baoji, Shaanxi, China.

**Abstract**: Low water solubility and poor intestinal permeability hinder the oral absorption of curcumin (CUR). To address this, we designed a core-shell structured nanoparticle based on nanodiamonds (NDs) and thiolated chitosan (TCS). First, D-α-tocopherol polyethylene glycol 1000 succinate (TPGS) covalently modified NDs were prepared and loaded with CUR (CUR@NDs-TPGS). N-acetylcysteine (NAC) was then coupled to chitosan (CS) to obtain positively charged CS-NAC, which electrostatically coated the negatively charged NDs-TPGS/CUR. Particle size (PS), zeta potential (ZP) and drug loading efficiency (DLE) were selected as screening indices to optimize the formulation and preparation process of CUR@NDs-TPGS/CS-NAC via single-factor experiments. The results showed that after coating with CS-NAC, the PS of optimized CUR@NDs-TPGS/CS-NAC increased from 183.63±5.24 nm to 245.24±3.95 nm, the ZP value flipped from -25.47±1.36 to +25.81±1.06 and the DLE value decreased slightly. Moreover, the nanoparticles adopted a spherical morphology and the cumulative release percentage of the nanocomplexes within 24 h decreased from 35.69% to 25.54% after coating. CUR@NDs-TPGS/CS-NAC remained stable within 48 h in simulated intestinal fluid. Mucin adsorption, GI retention and oral absorption of CUR@NDs-TPGS/CS-NAC were further enhanced compared to CUR@NDs-TPGS. These findings suggest that CUR@NDs-TPGS/CS-NAC is a promising carrier for oral delivery of CUR.

**Keywords**: TPGSylated nanodiamonds; thiolated chitosan; oral drug delivery; curcumin

*Submitted on 07-08-2024 – Revised on 04-03-2025 – Accepted on 14-04-2025*

## INTRODUCTION

Curcumin (CUR) is a hydrophobic polyphenolic substance derived from the rhizomes of the *Curcuma longa*, exhibits diverse pharmacological properties such as anti-tumor (Yan *et al*., 2024), anti-inflammatory (Serini *et al*., 2025), antibacterial (Shome *et al*., 2022), anti-oxidation (Li *et al*., 2020) and neuroprotective effects (Subedi and Gaire, 2021). However, CUR is a Biopharmaceutics Classification System (BCS) class IV drug with low water solubility, poor mucosal permeability and instability under neutral, alkaline and light exposure (Chen *et al*., 2020). How to use pharmaceutical methods to break the above barriers of drug delivery and effectively improve the bioavailability of CUR is the key to solve the problem of its poor druggability.

The two main strategies to address the oral absorption challenges of CUR involve improving solubility and enhancing intestinal permeability. Nano-formulations demonstrate distinct advantages over traditional drug delivery systems through their small particle size and large surface area. To improve CUR's oral bioavailability, researchers have developed various nano-drug delivery strategies, including nano suspensions (Jiang *et al*., 2020), liposomes (Laurindo *et al*., 2023), polymer micelles (Gupta *et al*., 2020) and nano lipid carriers (Velderrain-Rodríguez *et al*., 2023).

Nanodiamonds (NDs), the most recent member of the carbon family, have many advantages for drug delivery including small size, simple surface modification, excellent adsorption properties and biocompatibility (Rehman *et al*., 2020; Perevedentseva *et al*., 2021; Díez-Pascual, 2021). In recent years, researchers have developed a number of functionalized NDs to delivery proteins (Zhang *et al*., 2020), nucleic acids (Tripathy *et al*., 2023; Majer *et al*., 2024) and chemical drugs (Cui *et al*., 2023; Su *et al*., 2024). In our previous study, a D-α-tocopherol polyethylene glycol 1000 succinate (TPGS) covalently conjugated NDs system (NDs-TPGS) was developed to improve the oral bioavailability of CUR (Liu *et al*., 2020). Although the nanocomplexes we constructed could improve the solubility, intestinal retention and permeability of the drug, the nanoparticles still need to be further modified to ensure that the drug can bypass the stomach, remain in the small intestine for a long time and enter the blood circulation through the intestinal mucosa.

Thiolated chitosan (TCS) is a kind of modified chitosan (CS) with free thiol groups prepared by covalently linking thiol groups to amino groups on CS. The introduction of thiol groups not only solves the solubility problem of CS, but also endows the polymer with enhanced mucoadhesive properties and mucus layer permeability (Federer *et al*., 2021). TCS can be anchored in the mucus layer by forming stable disulfide bonds with cysteine-rich regions in the

**Corresponding author:* e-mail: liudandan1124@126.com, 724643957@qq.com

mucus layer, subsequently penetrating to the mucus layer base through reversible disulfide bond exchange reactions (Bernkop-Schnürch, 2005). It can also open tight junctions between cells and facilitate drug penetration (Pratap-Singh *et al*., 2023). N-acetylcysteine (NAC), an acetylated derivative of L-cysteine, is a safe and effective thiolation reagent. NAC can open tight junctions and promote drug penetration by inhibiting protein tyrosine phosphatases, while also disrupting mucin disulfide bonds to reduce mucin fiber cross-linking, thereby enhancing drug penetration (Sheng *et al*., 2022).

In this research, we constructed a CUR loaded core-shell structured nanoparticle (CUR@NDs-TPGS/CS-NAC) through electrostatic. Firstly, acetylated NDs and TPGS were covalently coupled to form NDs-TPGS and loaded with CUR. Then, CS was covalently modified with NAC to obtain positively charged TCS, which was coated with negatively charged NDs-TPGS/CUR through electrostatic interaction. The schematic illustration of the preparation process of CUR@NDs-TPGS/CS-NAC was shown in Fig.1.The single-factor experiment was employed to optimize the formulation and preparation parameters of CUR@NDs-TPGS/CS-NAC. After that, the properties of the optimized nanoparticle such as particle size (PS), zeta potential (ZP), morphology and stability were characterized. Furthermore, the mucoadhesive efficiency of the nanoparticle was estimated using mucin adsorption and ex vivo fluorescence imaging study.

## MATERIALS AND METHODS

### *Materials*

CUR was obtained from Aladdin (Shanghai, China). NDs were acquired from Nanjing XFNANO Materials Tech Co., Ltd. (Nanjing, China). TPGS was from Macklin Biochemical Co., Ltd. (Shanghai, China). CS-NAC, containing free sulfhydryl groups (489.6 ± 13.5 μmol/g) , was synthesized via carbodiimide-mediated covalent conjugation of CS with NAC, as detailed in our prior work (Liu *et al*., 2016). Mucin type III was purchased from Sigma-Aldrich (St. Louis, MO, USA). All other chemicals were of analytical or chromatographic quality.

### *Animals*

Male Kunming mice, with a weight of 20 ± 2 g, were acquired from the Laboratory Animal Center of Shenyang Pharmaceutical University (Shenyang, China). All animal studies were carried out in compliance with the guidelines of Laboratory Animal Care and were sanctioned by the Animal Ethical Committee of Shenyang Pharmaceutical University (SYPUIACUC-C-5-16-207).

### *Fabrication and optimization of the formulations*

*Preparation of TPGSylated NDs*

In order to prepare CUR loaded NDs particles, TPGSylated NDs (NDs-TPGS) were synthesized via covalent conjugation of TPGS to acylated NDs. Briefly, pristine NDs were first carboxylated by acid treatment ($H_2SO_4/HNO_3$, 3:1 v/v, 60°, 24 h), followed by acylation with oxalyl chloride in the presence of DMF. The resulting NDs-COCl were then reacted with TPGS (50 mg) in DMF at 100° overnight. The final product was purified by centrifugation, washed with distilled water and lyophilized. Detailed synthesis steps and characterization data of NDs-TPGS can be referred to our previously published work (Liu *et al*., 2020).

### *Preparation of CUR loaded nanocomplexes*

CUR loaded NDs-TPGS (CUR@NDs-TPGS) were prepared as follows. NDs-TPGS ethanol dispersion (5 mg/mL) was subjected to probe sonication (SCIENTZ-32 IID, Scientz Biotechnology Co., Ltd., Ningbo, China) at different ultrasonic powers for different durations. A CUR acetone solution with various concentrations (2 mL) was added dropwise and sonicated for another 30 min. The mixture was then evaporated into dryness under reduced pressure. The resultant CUR@NDs-TPGS was resuspended in 10 mL of distilled water by sonication for 10 min. To prepare CS-NAC coated CUR@NDs-TPGS (CUR@NDs-TPGS/CS-NAC), the NDs dispersion was added to the same volume of polymer solution with different concentrations (0.1%, 0.3% and 0.5%, w/v) under vigorous stirring, followed by incubation for a specified time at room temperature. CUR suspension, the negative control, was prepared by adding a CUR acetone solution (1.5 mg/mL, 2mL) into 10 mL 0.5% CMC-Na solution, followed by sonication for 30 min. Coumarin-6 (Cou-6)-labeled particles were prepared similarly, except that Cou-6 (1 mg/mL, 2 mL) was incorporated into the ND carriers instead of the CUR solution.

### *Optimization of the formulation and preparation parameters*

In this study, a single-factor experiment was employed to optimize the formulation and preparation parameters of CUR@NDs-TPGS/CS-NAC (Lin *et al*., 2022). While holding other factors constant, the influence of ultrasonic intensity, ultrasonic duration, the amount of drug added, CS-NAC concentration and the polymer coating time on the physicochemical characterization of the preparations was studied, respectively.

### *Physicochemical characterization of NDs preparations*

*Particle size and zeta potential*

The particle size (PS), size distribution (polydispersity index, PDI) and surface charge (zeta potential, ZP) were characterized using a Nano ZS90 dynamic light scattering instrument (Malvern, UK). The measurements were carried out in triplicate at room temperature.

### *Drug loading*

To characterize drug loading efficiency (DLE, %), NDs preparations were analyzed by UV/vis measurements (UV-

2000, UNICO, USA) at 423 nm before and after centrifuged at 12,000 rpm for 10 min to determine the total amount of CUR and drug loss. DLE was calculated using the following formula:

$$\text{DLE} \quad (\%) \quad = \quad \frac{W_T - W_F}{W_T} \times 100$$

where $W_T$ and $W_F$ are the weights of total amount of CUR in the preparation and the unencapsulated drug in the supernatant, respectively.

***Surface morphology***

Morphological analysis of blank NDs carriers and drug loaded ones was performed by JEM-1200EX microscope (JEOL, Tokyo, Japan). The procedure was as follows: the NDs dispersion was diluted to an appropriate concentration and cast dropwise onto a copper grid coated with an amorphous carbon film. After being desiccated at room temperature, the samples were negatively stained with 2% phosphotungstic acid and examined under the transmission electron microscope (TEM) to observe the morphology.

***Release behavior study***

The release of drug loaded NDs was investigated using the dialysis bag technique (MWCO 8000–14,000). Nanoparticles equivalent to 1mg of CUR were transferred to dialysis bags, immersed in 250 mL simulated gastric fluid (pH 1.2, 1.0% Tween 80) for the first 2h, followed by transfer to into 250 mL of simulated intestinal fluid (pH 6.8, 1.0% Tween 80) for 22h. To simulate the release environment *in vivo* after oral administration, samples were incubated at 37 ± 0.5 °C with a shaking speed of 100 rpm in the dark (Liu *et al*., 2016). At the desired time points, 1 mL of the release medium was withdrawn and immediately replaced with an equal volume of fresh medium. After centrifugation at 12,000 rpm for 10 min, the samples were analyzed by HPLC.

***Colloidal stability***

The *in vitro* colloidal stability of CUR@NDs-TPGS and CUR@NDs-TPGS/CS-NAC were evaluated by monitoring the variation in PS values (Lim *et al*., 2016). To conduct the experiment, 100 μL NDs complexes were diluted with 5 mL simulated intestinal fluids (pH 6.8). After the samples were withdrawn at predetermined time points (0, 12, 24 and 48h), the PS values were determined immediately.

***Mucin adsorption study***

In this study, the adhesion property of NDs preparations to intestinal mucosa was indirectly predicted by measuring the mucin adsorption capacity of NDs nanocomplexes over specific time intervals (Takeuchi *et al*., 2018). First, the CUR suspension and NDs dispersions (3 mg/mL) were mixed with an equal volume type β mucin solution (1 mg/mL or 2 mg/mL), vortexed and incubated at 37° for 12h. After adsorption for 1, 3 and 6 h, samples were collected, centrifuged for 10 min at 10,000 rpm. The supernatant was sampled and mixed with an equal volume of periodic acid solution, incubated in a 37° water bath for 2 h and then analyzed colorimetrically using periodic acid/Schiff (PAS) staining. The amount of unabsorbed mucin was quantified using an ultraviolet spectrophotometer at 560 nm. The adsorbed mucin amount was calculated by subtracting the supernatant mucin concentration from the initial amount. To prepare a standard curve, mucin standards (50, 100, 150, 300 and 600 μg/mL) were processed identically.

***Ex vivo fluorescence imaging***

To study the gastrointestinal (GI) retention and tissue distribution in the mice after oral administration, fluorescence intensity in isolated organs was investigated by *in vivo* imaging instrument (Carestream FX Pro, USA). The Kunming mice were deprived of food overnight with free access to water prior to the study. Free Cou-6, Cou-6@NDs-TPGS and Cou-6@NDs-TPGS/CS-NAC were administered to the mice with a Cou-6 dosage of 3 mg/kg by gavage respectively. The mice were sacrificed at 0.5, 2, or 5 h post-administration and the GI tract was collected for fluorescence imaging. Major organs, including the heart, liver, spleen, lung and kidney, were also collected to evaluate tissue drug distribution.

## STATISTICAL ANALYSIS

All experiments were conducted in triplicate to ensure reproducibility. Data are expressed as the mean ± SD. The data were analyzed using independent sample t tests. Statistical analyses were performed using SPSS 26.0 (IBM Corp., Armonk, NY, USA). *P* value less than 0.05 and 0.01 were considered as statistically significant and highly statistically significant, respectively.

## RESULTS

***The effect of ultrasonic power intensity on the properties of CUR@NDs-TPGS***

As shown in table.1, the PS of CUR@NDs-TPGS decreased significantly with the increase of ultrasonic power, particularly from 240 W to 360 W (26.9% reduction, $P < 0.01$). Beyond 360 W, PS reduction plateaued. Thus, 360 W was selected as the optimal ultrasonic power.

***The influence of ultrasonic duration on the properties of CUR@NDs-TPGS***

According to table. 2, the PS of the NDs particles decreased significantly ($P < 0.01$) with the extension of ultrasonic time. However, when the duration exceeded 30 min, no significant improvements were observed in PS, ZP, or DLE under the tested conditions. In addition, when PS decreases, particle surface area increased, DLE and absolute ZP value increased. This balance between particle quality and preparation efficiency supports the selection of 30 min as the optimal ultrasonic duration.

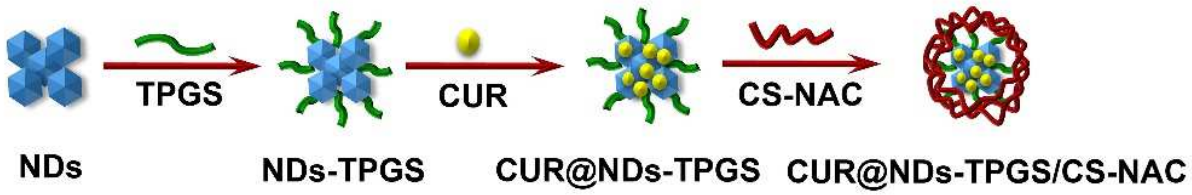


**Fig. 1**: Schematic illustration of the preparation process of CUR@NDs-TPGS/CS-NAC

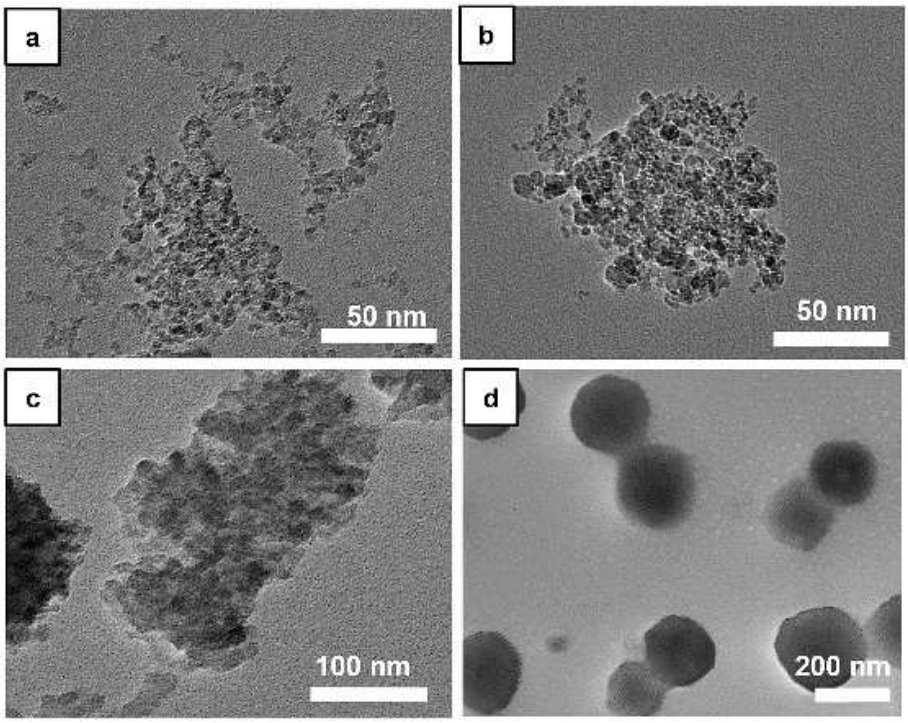


**Fig. 2**: TEM images of ND-COOH, ND-TPGS, CUR@NDs-TPGS, and CUR@NDs-TPGS/CS-NAC

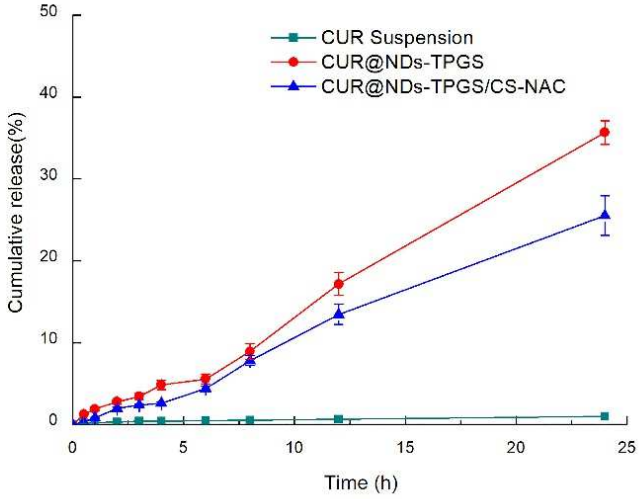


**Fig. 3**: *In vitro* release profile of CUR from ND complexes (Mean ± SD, n=3).

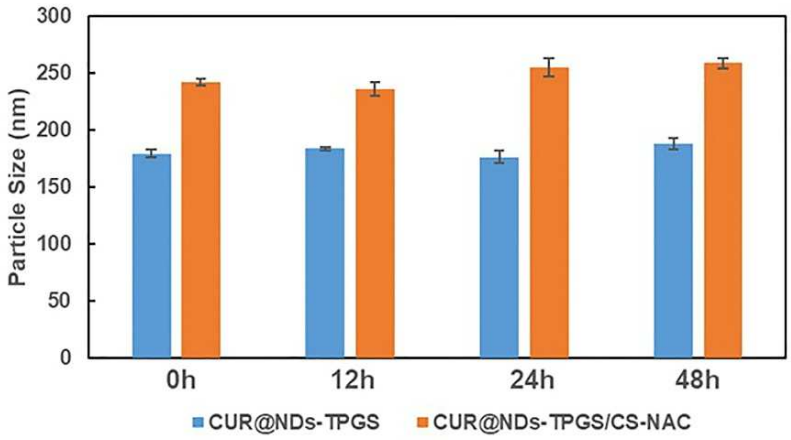


**Fig. 4**: Colloidal stability of CUR@NDs-TPGS and CUR@NDs-TPGS/CS-NAC in simulated intestinal fluid at different time points (Mean ± SD, n=3).

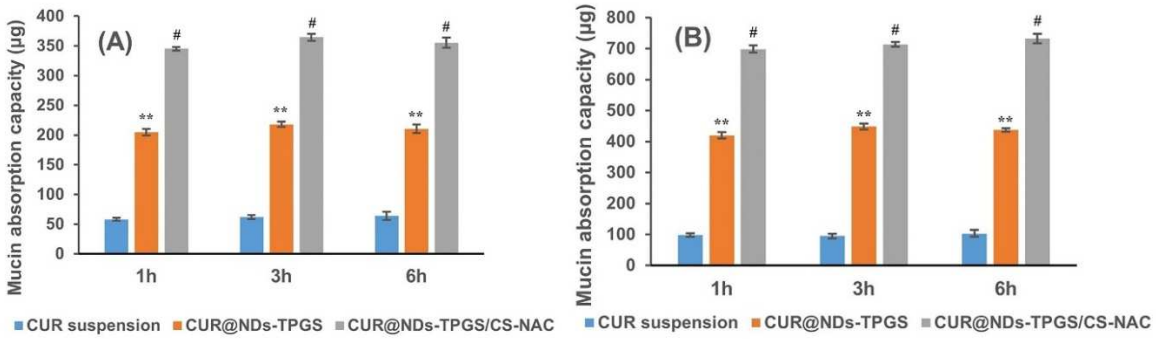


**Fig. 5**: Mucin absorption of CUR preparations after interaction with different concentrations of mucin protein (Mean ± SD, n=3): (A) at 1mg/mL; (B) at 2mg/mL. $^{**}P<0.01$ compared with CUR suspension, $^{\#}P<0.01$ compared with CUR@ND-TPGS.

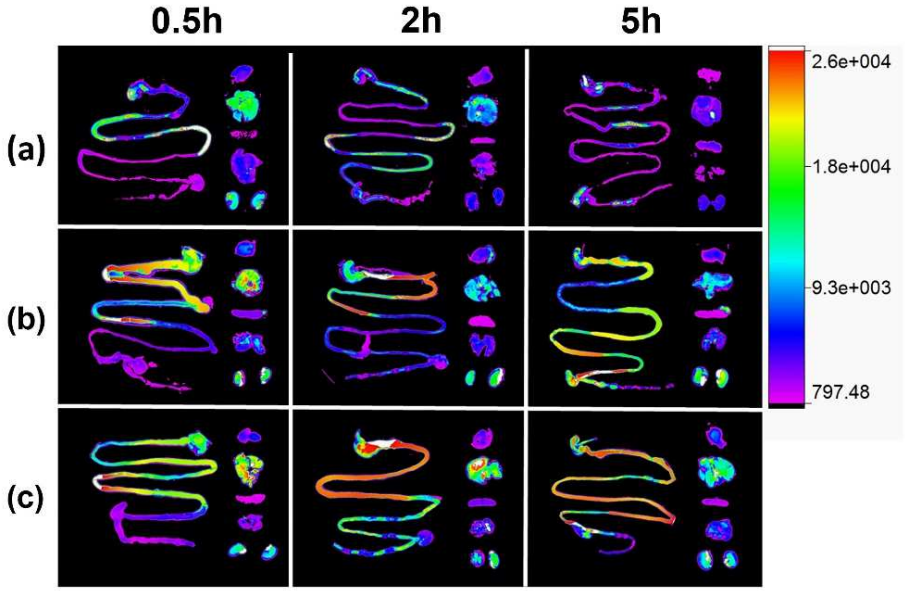


**Fig. 6**: *Ex vivo* fluorescence images of GI tract and major organs harvested from the mice after 0.5, 2, and 5 h after oral administration: (a) Cou-6 solution, (b) Cou-6@NDs-TPGS, and (c) Cou-6@NDs-TPGS/CS-NAC.

**Table 1**: The effect of ultrasonic power on the properties of CUR@NDs-TPGS (n=3)

| Ultrasonic power (W) | PS (nm) | ZP (mV) | DLE (%) |
|---|---|---|---|
| 240 | 251.28±4.74 | -23.45±2.35 | 77.13±7.62 |
| 360 | 183.63±5.24$^{\#\#}$ | -25.47±1.36 | 85.09±2.53$^{*}$ |
| 480 | 172.83±2.60$^{\#\#}$ | -26.33±4.09 | 86.54±5.48$^{*}$ |

$^{\#\#}P < 0.01$ compared with the ultrasonic power at 240 W, $^{*}P < 0.05$ compared with the ultrasonic power at 240 W.

**Table 2**: The influence of ultrasonic duration on the properties of CUR@NDs-TPGS (n=3)

| Ultrasonic duration (min) | PS (nm) | ZP (mV) | DLE (%) |
|---|---|---|---|
| 10 | 293.28±8.05 | -20.68±3.42 | 68.13±7.62 |
| 30 | 183.63±5.24$^{\#\#}$ | -25.47±1.36 | 85.09±2.53$^{\#}$ |
| 60 | 166.47±4.16$^{\#\#}$ | -26.33±4.09 | 84.71±3.64$^{\#}$ |

$^{\#}P < 0.05$ compared with the ultrasonic duration was 10 min, $^{\#\#}P < 0.01$ compared with the ultrasonic duration was 10 min.

**Table 3**: The impact of CUR addition amount on the properties of CUR@NDs-TPGS (n=3)

| CUR added (mg) | PS (nm) | ZP (mV) | DLE (%) |
|---|---|---|---|
| 1 | 174.87±6.82 | -16.27±2.73 | 79.58 ± 4.69 |
| 3 | 183.63±5.24$^{\#\#}$ | -25.47±1.36$^{\#}$ | 85.09±2.53$^{\#}$ |
| 5 | 269.17±11.38$^{**}$ | -28.92±5.09$^{\#}$ | 83.32 ± 8.32$^{\#}$ |

$^{\#}P < 0.05$ compared with the input amount of CUR was 1 mg, $^{\#\#}P < 0.01$ compared with the input amount of CUR was 1 mg, $^{**}P < 0.01$ compared with the input amount of CUR was 3mg.

**Table 4**: The effect of CS-NAC concentration on PS, ZP and DLE of the preparations (n=3)

| The concentration of CS-NAC (%) | PS (nm) | ZP (mV) | DLE (%) |
|---|---|---|---|
| 0.1 | 217.16±2.11 | 19.08±0.84 | 76.23±1.36 |
| 0.3 | 245.24±3.95$^{\#}$ | 25.81±1.06$^{\#\#}$ | 80.33±3.77 |
| 0.5 | 291.49±7.17$^{**}$ | 36.45±3.72$^{*}$ | 83.54±5.48 |

$^{\#}P < 0.05$ compared with the concentration of CS-NAC was 0.1%, $^{\#\#}P < 0.01$ compared with the concentration of CS-NAC was 0.1%, $^{*}P < 0.05$ compared with the concentration of CS-NAC was 0.3%, $^{**}P < 0.01$ compared with the concentration of CS-NAC was 0.3%.

**Table 5**: The impact of CS-NAC coating time on PS, ZP and DLE of the preparations (n=3)

| Coating time (h) | PS (nm) | ZP (mV) | DLE (%) |
|---|---|---|---|
| 0.5 | 268.98 ± 2.46 | 17.07 ± 2.11 | 81.54±5.31 |
| 1.0 | 245.24±3.95$^{\#}$ | 25.81±1.06$^{\#}$ | 80.33±3.77 |
| 1.5 | 284.17 ±4.09$^{\#\#,**}$ | 33.26 ± 3.54$^{\#,*}$ | 74.66±5.52$^{\#}$ |

$^{\#}P < 0.05$ compared with the coating time of 0.5h, $^{\#\#}P < 0.01$ compared with the coating time of 0.5h, $^{*}P < 0.05$ compared with the coating time of 1.0h, $^{**}P < 0.01$ compared with the coating time of 1.0h

**Table 6**: Pharmaceutical properties of the optimized formula (mean ± SD, n = 3)

| Properties | ND-TPGS | CUR@NDs-TPGS | CUR@NDs-TPGS/CS-NAC |
|---|---|---|---|
| PS (nm) | 154.92±9.66 | 183.63±5.24$^{\#\#}$ | 245.24±3.95$^{\#\#, **}$ |
| PDI | 0.15±0.01 | 0.19±0.01$^{\#}$ | 0.17±0.01$^{\#}$ |
| ZP (mV) | -12.14±2.05 | -25.47±1.36$^{**}$ | 25.81±1.06$^{**}$ |
| DLE (%) | - | 85.09±2.53 | 80.33±3.77 |

$^{\#}P < 0.05$ compared with ND-TPGS, $^{\#\#}P < 0.01$ compared with ND-TPGS, $^{*}P < 0.05$ compared with CUR@NDs-TPGS, $^{**}P < 0.01$ compared with CUR@NDs-TPGS, respectively.

***The impact of CUR addition amount on the properties of CUR@NDs-TPGS***

As shown in table.3, when other factors were fixed, the PS and absolute value of ZP increased with higher drug input, while the DLE first increased and then decreased. Since the CUR acetone solution is negatively charged, table.3 shows that the absolute value of ZP increased with more drugs entering the carrier. The addition amount of CUR was set at 3mg.

***The effect of CS-NAC concentration on the properties of the preparations***

As shown in table.4, the PS and ZP of CUR@NDs-TPGS/CS-NAC exhibited a significant CS-NAC concentration-dependent increase ($p < 0.05$) when other factors were fixed. There is a positive correlation between PS and polymer concentration (increasing from 217.16 nm at 0.1% to 291.49 nm at 0.5%, $p < 0.01$) and the more positive polymers wrapped, the greater the ZP of the preparation (from 19.08 mV at 0.1% to 36.45 mV at 0.5%, $p < 0.01$). However, when CS-NAC concentration exceeded 0.3%, further PS growth (291.49 nm vs. 245.24 nm, $p < 0.01$) raised concerns about nanoparticle aggregation, while the DLE improvement plateaued (only a 3.21% increase from 0.3% to 0.5%). Considering the balance between colloidal stability and DLE, the optimal CS-NAC concentration was determined as 0.3%.

***The impact of CS-NAC coating time on the properties of the preparations***

As shown in table. 5, with other factors fixed and unchanged, the PS of CUR@NDs-TPGS/CS-NAC initially decreased and then increased with the extension of CS-NAC coating time, while the ZP increased and the DLE gradually decreased. At 1 h, the PS decreased ($p < 0.05$) and the ZP increased ($p < 0.05$), while DLE slightly decreased ($p > 0.05$). With the further extension of coating time, the coating amount of CS-NAC on the particle surface continued to increase, so a larger PS and ZP were obtained. However, further extension to 1.5 h would lead to the loss of drug in the nanoparticles, thus the coating time was determined as 1 h.

***Physicochemical characterization of optimized preparations***

After optimizing the preparation process and formulation of NDs, the properties of the nanocomplexes such as PS, ZP, morphology and stability were characterized. According to table.6, the PS of NDs-TPGS increased progressively after drug loading and CS-NAC coating, while the PDI increased slightly. The absolute ZP value increased significantly post drug loading and the surface charge reversed from negative to positive after CS-NAC coating, confirming successful drug incorporation and carrier modification. π–π stacking interactions between benzene rings of NDs-TPGS and aromatic groups of CUR molecules contributed to drug loading. Compared to CUR@NDs-TPGS, CS-NAC coating caused a slight decrease in the DLE. fig. 2 illustrates the microstructure of NDs complexes. ND-COOH exhibited irregular aggregates of multiple monomers. Upon TPGS covalent modification, the aggregates thickened, forming nanoparticles with distinct NDs-rich and TPGS-rich regions. For CUR@NDs-TPGS, the blurred aggregate surface indicated successful drug loading. Electrostatic interactions enabled CUR@NDs-TPGS to be coated with positively charged CS-NAC. As shown in fig. 2d, the nanoparticles became regular spheres after coating.

*In vitro* release behavior of NDs complexes was studied under pH gradient conditions. The release medium was selected to simulate the *in vivo* environment and achieve sink conditions. CUR showed minimal release from its suspension (fig. 3). Upon successful formation of NDs complexes, drug release was significantly improved. NDs-TPGS acted as a repository to provide improved dissolution, stability and sustained release of CUR. After being coated with CS-NAC, the cumulative release percentage of the nanocomplexes within 24h was decreased from 35.69% to 25.54%.

It is essential to study the stability of nanocomposites in the GI environment, as changes in PS directly affect nanoparticle-mucosa interactions (Liu *et al*., 2019). According to fig. 4, CUR@NDs-TPGS and CUR@NDs-TPGS/CS-NAC remained stable for 48h, with no significant change in PS and no visible aggregates observed.

***Mucin adsorption***

A comparison of fig. 5 (A) and 4 (B) shows that the adsorbed mucin amount correlated with mucin concentration. As predicted, the CUR suspension exhibited the lowest mucin adhesion force. In contrast with the suspension group, the mucoadhesive force of CUR@NDs-TPGS was significantly improved ($P < 0.01$). According to fig. 5, mucin adsorption of CUR@NDs-TPGS/CS-NAC was further enhanced compared to CUR@NDs-TPGS ($P < 0.01$).

***The intestinal retention and tissue distribution of preparations***

The intestinal retention results are shown in fig. 6. For the Cou-6 solution group, the fluorescence was mainly concentrated in the upper and middle sections of the intestine at 0.5 h. At 2 h, it was gradually transported to the middle and lower sections. At 5 h, nearly no fluorescence was observed in the upper section of GI tract. For the Cou-6@NDs-TPGS group, the fluorescence intensity was the strongest at 0.5 h and mainly concentrated in the upper intestinal section. At 2 h, it remained in the upper and middle sections. At 5 h, fluorescence was distributed throughout the GI tract, with slightly stronger intensity in the middle and lower sections, indicating drug had been transported to the lower intestine. For the Cou-6@NDs-

TPGS/CS-NAC group, although a considerable amount of the drug had entered the upper gastrointestinal tract at 0.5 h, the fluorescence intensity in the upper section of the intestine further intensified at 2 h and the formulation was only transported to the middle and lower sections of the intestine at 5 h, with strong fluorescence still visible in the upper section of the intestine.

As shown in fig. 6, the right side of the GI tract displays the distributions of the formulations in the heart, liver, spleen, lung and kidney (from top to bottom). Improved intestinal retention significantly promoted the *in vivo* drug absorption. Fluorescence intensities in major organs followed the order: Cou - 6@NDs - TPGS/CS - NAC > Cou-6@NDs-TPGS > Cou-6 solution, with Cou-6 predominantly localized in the liver and kidneys.

## DISCUSSION

The uniform dispersion of NDs-TPGS is the premise of drug loading, so we systematically investigated the influence of ultrasonic power intensity on CUR@NDs-TPGS properties. Beyond 360 W, PS reduction plateaued, likely due to the saturation of cavitation effects. This finding aligns with prior studies demonstrating that ultrasonic cavitation generates transient high-energy microenvironments through bubble collapse, disrupting particle agglomeration (Yang *et al*., 2023). Strong cavitation-induced shear forces and microjets facilitate nanoparticle dispersion. However, excessive power leads to inefficient bubble formation and scattering attenuation, limiting further size reduction (Sabnis *et al*., 2022). The optimized PS at 360 W also improved DLE, which may be attributed to the enhanced surface area and reduced steric hindrance for drug encapsulation (Chen *et al*., 2017). Additionally, moderate ultrasonic treatment likely preserved nanoparticle stability by minimizing aggregation. These results validate our hypothesis that balanced ultrasonic intensity optimizes both particle dispersion and stability.

The influence of ultrasonic duration on the properties of CUR@NDs-TPGS was investigated. When the duration exceeded 30 min, no significant improvements were observed in PS, ZP, or DLE under the tested conditions. This plateau effect may arise from two competing mechanisms. On the one hand, prolonged sonication increases solution temperature, reducing surface tension and viscosity, which enhances cavitation efficiency. On the other hand, continuous cavitation depletes dissolved gases, raising the cavitation threshold and diminishing its effectiveness (Jiang *et al*., 2023). Therefore, insufficient cavitation at short durations fails to achieve optimal dispersion while prolonged sonication leads to cavitation saturation, limiting further PS reduction. Notably, excessive sonication may even induce particle aggregation due to thermal stress (Ni *et al*., 2024).

When other factors were fixed, the PS and absolute value of ZP increased with higher drug input, while the DLE first increased and then decreased. This may be because with the increase of CUR input amount, it is beneficial to the full contact between the nanocarrier and the drug, thus improving the adsorption capacity of the carrier for CUR and the size of the nanoparticle increased as more drugs were loaded. Beyond the saturation threshold of the nanocarrier's adsorption capacity, excess CUR disrupted the colloidal stability of the system, thus enlarging the PS and reducing the DLE (Stenzel, 2021).

The PS and ZP of CUR@NDs-TPGS/CS-NAC exhibited a significant CS-NAC concentration-dependent increase. This could be attributed to the fact that the larger the amount of CS-NAC in the system, the higher the probability of its contact with CUR@NDs-TPGS. This situation is more conducive to the polymer wrapping around the surface of CUR@NDs-TPGS via electrostatic interactions. In addition, with the increase of polymer concentration, the viscosity of the system increased and the leakage of the drug was effectively inhibited, so the DLE increased (Briggs *et al*., 2022).

The PS of CUR@NDs-TPGS/CS-NAC initially decreased and then increased with the extension of CS-NAC coating time, while the ZP increased and the DLE gradually decreased. This may be because at 0.5 h, less CS-NAC was coated on the surface of nanoparticles and the coating layer was relatively loose. At 1 h, the coating amount increased and the coating layer became denser. With the further extension of coating time, the coating amount of CS-NAC on the particle surface continued to increase, so a larger PS and ZP were obtained. We hypothesize that excessive coating duration induced polymer over-adsorption on the particle surface, triggering aggregation and partial drug leakage.

After being coated with CS-NAC, the cumulative release percentage of the nanocomplexes within 24h was decreased from 35.69% to 25.54%, which may promote passive diffusion and prevents overwhelming cell-uptake mechanisms (Ramalingam *et al*., 2015). Given CUR's poor solubility and absorption, the CS-NAC coating shields against premature degradation in the gut, enhancing its intact absorption into the bloodstream (Ma *et al*., 2019).

The GI mucus layer is a critical barrier to oral drug absorption (Oransa *et al*., 2022). In our study, mucoadhesive efficiency of CUR preparations was evaluated by measuring the adsorption of mucin on the formulations. As predicted, the CUR suspension exhibited the lowest mucin adhesion force, attributed to its larger PS and the electrostatic repulsion between the negatively charged particles and the mucus layer. In contrast with the suspension group, the mucoadhesive force of CUR@NDs-TPGS was significantly improved, which may be due to the

small size effect of the carrier, the significantly increased surface area, hydrogen bonding interaction and van der Waals forces. Mucin adsorption of CUR@NDs-TPGS/CS-NAC was further enhanced compared to CUR@NDs-TPGS. This is because positively charged CUR@NDs-TPGS/CS-NAC can generate strong electrostatic interactions with negatively charged mucins (Shin *et al*., 2021). Additionally, CS-NAC forms strong disulfide bonds with the cysteine group of mucins, further enhancing the adhesion of the preparation (Liu *et al*., 2016). Therefore, CUR@NDs-TPGS/CS-NAC is anticipated to prolong intestinal retention of the drug delivery system and augment CUR bioavailability.

To study the retention and tissue distribution of each preparation in the GI tract of mice after administration, the fluorescence distribution of Cou-6 in the isolated GI tract and principal organs was investigated using an in vivo imaging device. Among the preparations, Cou-6@NDs-TPGS/CS-NAC exhibited the longest GI retention. This is because CS-NAC on the nanoparticle surface possesses a strong mucus adhesion property and its positive charge tends to adhere to the negatively charged intestinal wall cell membrane, thereby increasing nanoparticle-intestine interaction time. CS-NAC can also form strong disulfide bonds with mucin cysteine groups in the intestinal mucus layer, further enhancing the adhesion of the formulation and effectively prolonging the interaction time of nanoparticles with the intestine (Sudhakar *et al*., 2020). Longer retention maintains a relatively high drug concentration, forms a concentration gradient and facilitates passive diffusion and absorption of Cou-6.

## CONCLUSION

In this study, a novel core-shell structured nanoparticle based on TPGSylated NDs and CS-NAC was developed to solve the problem of efficient oral CUR delivery. The preparations were fabricated by first dispersing NDs-TPGS via ultrasonic homogenization, followed by CUR adsorption and coating with CS-NAC. Single factor investigation revealed that the PS, ZP and DLE of the preparations were obviously affected by ultrasonic intensity, duration, drug addition amount, CS-NAC concentration and TCS coating duration. Post coating, the PS of CUR@NDs-TPGS increased and the ZP reversed from negative to positive. While CUR@NDs-TPGS exhibited irregular aggregates, the coated nanoparticles exhibited a regular spherical morphology. In addition, the *in vitro* release of CUR could be significantly improved after incorporation into NDs nanoparticles and the release rate of CUR@NDs-TPGS/CS-NAC was slower than CUR@NDs-TPGS. Both NDs preparations showed good colloidal stability in simulated intestinal fluid. Mucin adsorption, GI retention and oral absorption of CUR@NDs-TPGS/CS-NAC was further enhanced compared to CUR@NDs-TPGS. These results collectively demonstrate that CUR@NDs-TPGS/CS-NAC possesses a series of promising properties for facilitating the oral delivery of CUR.

## ACKNOWLEDGMENTS

This work was supported by the Liaoning Provincial Natural Science Foundation Program (2024-MS-182), the Basic Research Projects in Higher Education Institutions (Key Projects) of the Liaoning Provincial Department of Education (LJ212411430010), Liaoning Provincial Department of Education Science and Technology Innovation Team Project (LJ222411430018) and the Pharmaceutical Cleaner Production and Industrialization Innovation Team of Liaoning Institute of Science and Technology (XKT202304).

***Conflicts of interest***

The authors declare no conflicts of interest.

## REFERENCES

Briggs F, Browne D and Asuri P (2022). Role of polymer concentration and crosslinking density on release rates of small molecule drugs. *Int. J. Mol. Sci.*, **23**(8): 4118.

Chen W, Palazzo A, Hennink WE and Kok RJ (2017). Effect of particle size on drug loading and release kinetics of gefitinib-loaded PLGA microspheres. *Mol. Pharm.*, **14**(2):459-467.

Chen Y, Lu Y, Lee RJ and Xiang G (2020). Nano encapsulated curcumin: And its potential for biomedical applications. *Int. J. Nanomedicine.*, **15**:3099–3120.

Cui J, Hu B, Fu Y, Xu Z and Li Y (2023). pH-Sensitive nanodiamond co-delivery of retinal and doxorubicin boosts breast cancer chemotherapy. *RSC. Adv.*, **13**(39): 27403-27414.

Díez-Pascual, AM (2021). Carbon-based nanomaterials. *Int. J. Mol. Sci.,* **22**(14): 7726.

Federer C, Kurpiers M and Bernkop-Schnürch A (2021). Thiolated chitosans: A multi-talented class of polymers for various applications. *Biomacromolecules*, **22**(1):24-56.

Gupta A, Costa AP, Xu X, Lee SL, Cruz CN, Bao Q and Burgess DJ (2020). Formulation and characterization of curcumin loaded polymeric micelles produced via continuous processing. *Int. J. Pharm*, **583**:119340.

Laurindo LF, de Carvalho GM, de Oliveira Zanuso B, Figueira ME, Direito R, de Alvares Goulart R, Buglio DS and Barbalho SM (2023). Curcumin-based nanomedicines in the treatment of inflammatory and immunomodulated diseases: an evidence-based comprehensive review. *Pharmaceutics*, **15**(1): 229.

Li L, Zhang X, Pi C, Yang H, Zheng X, Zhao L and Wei Y. (2020). Review of curcumin physicochemical targeting delivery system. *Int. J. Nanomedicine.*, **15**: 9799-9821.

Lim DG, Jung JH, Ko HW, Kang E and Jeong SH (2016). Paclitaxel-nanodiamond nanocomplexes enhance

aqueous dispersibility and drug retention in cells. *ACS. Appl. Mater. Interfaces.*, **8**(36): 23558-67.

Lin W, Li Y, Shi Q, Liao X, Zeng Y, Tian W, Xie X and Liu H (2022). Preparation and evaluation of bilayer-core osmotic pump tablets contained topiramate. *PLoS One*, **17**(2): e0264457.

Liu D, Qiao S, Cheng B, Li D, Chen J, Wu Q, Pan H and Pan W (2020). Enhanced oral delivery of curcumin via vitamin E TPGS modified nanodiamonds: A comparative study on the efficacy of non-covalent and covalent conjugated strategies. *AAPS Pharm. Sci. Tech.*, **21**(5):187.

Liu D, Li J, Pan H, He F, Liu Z, Wu Q, Bai C, Yu S and Yang X (2016). Potential advantages of a novel chitosan-N-acetylcysteine surface modified nanostructured lipid carrier on the performance of ophthalmic delivery of curcumin. *Sci. Rep.*, **6**: 28796.

Liu L, Yang H, Lou Y, Wu JY, Miao J, Lu XY and Gao JQ (2019). Enhancement of oral bioavailability of salmon calcitonin through chitosan-modified, dual drug-loaded nanoparticles. *Int. J. Pharm.*, **557**: 170-177.

Jiang H, Lu H, Zhou Y, Liu Y and Hao C (2023). High-efficiency degradation catalytic performance of a novel Angelica sinensis polysaccharide-silver nanomaterial for dyes by ultrasonic cavitation. *Ultrason. Sonochem.*, **93**: 106289.

Jiang L, Wang J, Jiang J, Zhang C, Zhao M, Chen Z, Wang N, Hu D, Liu X, Peng H and Lian M. (2020). Sonodynamic therapy in atherosclerosis by curcumin nanosuspensions: Preparation design, efficacy evaluation and mechanisms analysis. *Eur. J. Pharm. Biopharm.*, **146**:101-110.

Majer J, Kindermann M, Pinkas D, Chvatil D, Cigler P and Libusova L (2024). Cellular uptake and fate of cationic polymer-coated nanodiamonds delivering siRNA: A mechanistic study. *Nanoscale.,* **16**(5): 2490-2503.

Ma Z, Wang N, He H, Tang X (2019). Pharmaceutical strategies of improving oral systemic bioavailability of curcumin for clinical application. *J. Control. Release*, **316**:359-380.

Ni X, Chen C, Li R, Liu Q, Duan C, Wang X and Xu M (2024). Effects of ultrasonic treatment on the structure and functional characteristics of myofibrillar proteins from black soldier fly. *Int. J. Biol. Macromol.*, **278**(4): 135057.

Oransa HA, Boughdady MF and El-Sabbagh HM (2022). Novel mucoadhesive chitosomes as a platform for enhanced oral bioavailability of cinnarizine. *Int. J. Nanomedicine*, **17**: 5641-5660.

Perevedentseva E, Lin YC and Cheng CL (2021). A review of recent advances in nanodiamond-mediated drug delivery in cancer. *Expert. Opin. Drug. Deliv.*, **18**(3): 369-382.

Pratap-Singh A, Guo Y, Baldelli A and Singh A (2023). Mercaptonicotinic acid activated thiolated chitosan (MNA-TG-chitosan) to enable peptide oral delivery by opening cell tight junctions and enhancing transepithelial transport. *Sci. Rep.*, **13**(1): 17343.

Ramalingam P and Ko YT (2015). Enhanced oral delivery of curcumin from N-trimethyl chitosan surface-modified solid lipid nanoparticles: pharmacokinetic and brain distribution evaluations. *Pharm. Res.*, **32**(2): 389-402.

Rehman A, Houshyar S and Wang X (2020). Nanodiamond in composite: Biomedical application. *J. Biomed. Mater. Res. A.*, **108**(4): 906-922.

Sabnis SS, Singh SD and Gogate PR (2022). Improvements in azithromycin recrystallization using ultrasound for size reduction. *Ultrason. Sonochem.*, **83**:105922.

Serini S, Trombino S, Cassano R, Marino M and Calviello G (2025). Anti-inflammatory effects of curcumin-based nanoparticles containing α-linolenic acid in a model of psoriasis *in vitro*. *Nutrients*, **17**(4): 692.

Sheng Y, Sun X, Han J, Hong W, Feng J, Xie S, Li Y, Yan F, Li K and Tian B (2022). N-acetylcysteine functionalized chitosan oligosaccharide-palmitic acid conjugate enhances ophthalmic delivery of flurbiprofen and its mechanisms. *Carbohydr. Polym.*, **291**: 119552.

Shin GH and Kim JT (2021). Comparative study of chitosan and oligochitosan coatings on mucoadhesion of curcumin nanosuspensions. *Pharmaceutics*, **13**(12): 2154.

Shome S, Talukdar AD and Upadhyaya H (2022). Antibacterial activity of curcumin and its essential nanoformulations against some clinically important bacterial pathogens: A comprehensive review. *Biotechnol. Appl. Biochem.*, **69**(6): 2357-2386.

Stenzel MH (2021). The trojan horse goes wild: The effect of drug loading on the behavior of nanoparticles. *Angew. Chem. Int. Ed. Eng.l*, **60**(5): 2202-2206.

Su Y, Pan H, Wang J, Liu D and Pan W (2024). Eudragit S100 coated nanodiamond-based nanoparticles as an oral chemo-photothermal delivery system for local treatment of colon cancer. *Colloids. Surf. B. Biointerfaces*, **237**:113849.

Subedi L and Gaire BP (2021). Neuroprotective effects of curcumin in cerebral ischemia: Cellular and molecular mechanisms. *ACS. Chem. Neurosci.*, **12**(14): 2562-2572.

Sudhakar S, Chandran SV, Selvamurugan N and Nazeer RA (2020). Biodistribution and pharmacokinetics of thiolated chitosan nanoparticles for oral delivery of insulin *in vivo*. *Int. J. Biol. Macromol.*, **150**: 281-288.

Takeuchi I, Kamiki Y and Makino K (2018). Therapeutic efficacy of rebamipide-loaded PLGA nanoparticles coated with chitosan in a mouse model for oral mucositis induced by cancer chemotherapy. *Colloids. Surf. B. Biointerfaces*, **167**: 468-473.

Tripathy SP, Gupta SK, Nayak BP, Sahoo A, Das K, Singh VP, Verma S, Pal SK, Pal K and Ray SS (2023). Potential use of nucleic acids as a preceramic polymer to synthesize nanodiamond-embedded phosphate glass for hard tissue engineering. *ACS. Appl. Bio. Mater.*, **6**(10): 4138-4145.

Velderrain-Rodríguez G, Fontes-Candia C, López-Rubio A,

Martínez-Sanz M, Martín-Belloso O and Salvia-Trujillo L (2023). Polysaccharide-based structured lipid carriers for the delivery of curcumin: An *in vitro* digestion study. *Colloids. Surf. B. Biointerfaces*, **227**: 113349.

Yang M, Cao Y, Zhang Z, Guo J, Hu C, Wang Z and Du Y (2023). Low intensity ultrasound-mediated drug-loaded nanoparticles intravaginal drug delivery: An effective synergistic therapy scheme for treatment of vulvovaginal candidiasis. *J. Nanobiotechnology*, **21**(1): 53.

Yan S, Liao X, Xiao Q, Huang Q and Huang X (2024). Photostabilities and anti-tumor effects of curcumin and curcumin-loaded polydopamine nanoparticles. *RSC. Adv.*, **14**(20): 13694-13702.

Zhang Z, Li D, Ma X, Li X, Guo Z, Liu Y and Zheng S (2020). Carboxylated nanodiamond-mediated $NH_2$-PLGA nanoparticle-encapsulated fig polysaccharides for strongly enhanced immune responses *in vitro* and *in vivo*. *Int. J. Biol. Macromol.,* **165**(Pt A): 1331-1345.